

This discussion paper is/has been under review for the journal Atmospheric Chemistry and Physics (ACP). Please refer to the corresponding final paper in ACP if available.

Improved estimate of global dust radiative forcing using a coupled chemical transport-radiative transfer model

L. Zhang^{1,2,3}, Q. B. Li^{1,2}, Y. Gu^{1,2}, K. N. Liou^{1,2}, and B. Meland³

¹Department of Atmospheric and Oceanic Sciences, University of California, Los Angeles, CA, USA

²Joint Institute For Regional Earth System Science and Engineering, University of California, Los Angeles, CA 90095, USA

³Department of Mechanical Engineering, University of Colorado, Boulder, CO 80309, USA

Received: 28 November 2012 – Accepted: 9 January 2013 – Published: 23 January 2013

Correspondence to: L. Zhang (li.zhang@colorado.edu.edu)

Published by Copernicus Publications on behalf of the European Geosciences Union.

ACPD

13, 2415–2456, 2013

Improved estimate of global dust radiative forcing

L. Zhang et al.

Title Page

Abstract

Introduction

Conclusions

References

Tables

Figures



Back

Close

Full Screen / Esc

Printer-friendly Version

Interactive Discussion



Abstract

Atmospheric mineral dust particles exert significant direct radiative forcings and are critical drivers of climate change. Here, we use the GEOS-Chem global three-dimensional chemical transport model (3-D CTM) coupled online with the Fu-Liou-Gu (FLG) radiative transfer model (RTM) to investigate the dust radiative forcing and heating rates based on different dust vertical profiles. The coupled calculations using a realistic dust vertical profile simulated by GEOS-Chem minimize the physical inconsistencies between 3-D CTM aerosol fields and the RTM. The use of GEOS-Chem simulated aerosol optical depth (AOD) vertical profiles as opposed to the FLG prescribed AOD vertical profiles leads to greater and more spatially heterogeneous changes in estimated radiative forcing and heating rate produced by dust. Both changes can be attributed to a different vertical structure between dust and non-dust source regions. Values of the dust AOD are much larger in the middle troposphere, though smaller at the surface when the GEOS-Chem simulated AOD vertical profile is used, which leads to a much stronger heating rate in the middle troposphere. Compared to FLG vertical profile, the use of GEOS-Chem vertical profile reduces the solar radiative forcing effect by about $0.2\text{--}0.25\text{ W m}^{-2}$ and the Infrared (IR) radiative forcing over the African and Asia dust source regions by about $0.1\text{--}0.2\text{ W m}^{-2}$. Differences in the solar radiative forcing at the surface between using the GEOS-Chem vertical profile and the FLG vertical profile are most significant over the Gobi desert with a value of about 1.1 W m^{-2} . The radiative forcing effect of dust particles is more pronounced at the surface over the Sahara and Gobi deserts by using FLG vertical profile, while it is less significant over the downwind area of Eastern Asia.

1 Introduction

Mineral dust produced by the wind erosion of dry soil particles at the land surface has been recognized as a leading contributor to the global total aerosol loading (Andreas,

ACPD

13, 2415–2456, 2013

Improved estimate of global dust radiative forcing

L. Zhang et al.

[Title Page](#)

[Abstract](#)

[Introduction](#)

[Conclusions](#)

[References](#)

[Tables](#)

[Figures](#)

◀

▶

◀

▶

[Back](#)

[Close](#)

[Full Screen / Esc](#)

[Printer-friendly Version](#)

[Interactive Discussion](#)



1995; Tegen et al., 1997; Miller et al., 2006). Quantifying the impact of mineral dust on radiative forcing is important to understanding past climate and is necessary for the projection of future climate changes (IPCC, 2007). Model studies have suggested that the direct radiative forcing of dust on a regional and global scale may be comparable

5 to, or even exceed, the forcing by anthropogenic aerosols (Tegen and Fung, 1995; Li et al., 1996; Sokolik and Toon, 1996; Tegen et al., 1996). Using a radiative transfer model embedded in a general circulation model, Tegen et al. (1996) found that the dust particles from disturbed soils cause a decrease in net global average radiative forcing of about 1 W m^{-2} at the surface over all.

10 The optical and physical properties (shape, size distribution and refractive index) of dust particles as well as their vertical distribution constitute the basic parameters in determining radiative forcing and the subsequent feedback to dynamic and climate systems. The vertical distribution of aerosols is especially important as they modify the vertical profile of radiative heating in the atmosphere (e.g. Léon et al., 2002; Won et al., 15 2004; Ramanathan et al., 2007; Johnson et al., 2008), thereby changing atmospheric stability and convection (McFarquhar and Wang, 2006). In addition, it also influences the radiative effect at the top of the atmosphere (TOA), especially when aerosols have strong absorption of solar radiation (Meloni et al., 2005; Gadhavi and Jayaraman, 2006; Johnson et al., 2008). The vertical distribution of dust also plays an important role in 20 serving as cloud condensation nuclei (Li et al., 2011). Moreover, their positions relative to cloud cover would impact on radiative transfer in different ways.

In the evaluation of the radiative impact of dust particles, the critical concern is the uncertainty in the observed vertical structure of the dust distributions (Hamonou et al., 1999). A number of field programs have been carried out to measure the vertical distribution 25 of aerosols, including the Dust and Biomass-burning Experiment (DABEX), Tropospheric Aerosol Radiative Forcing Observation Experiment (TARFOX), and Puerto Rico Dust Experiment (PRIDE) (Hueber et al., 1998; Russell et al., 1999; Maring et al., 2003; Johnson et al., 2008). These ground-based and/or aircraft measurements have provided valuable information, but are limited in spatial and temporal coverage. The

[Title Page](#)

[Abstract](#)

[Introduction](#)

[Conclusions](#)

[References](#)

[Tables](#)

[Figures](#)

◀

▶

◀

▶

[Back](#)

[Close](#)

[Full Screen / Esc](#)

[Printer-friendly Version](#)

[Interactive Discussion](#)



Improved estimate of global dust radiative forcing

L. Zhang et al.

space borne lidar systems, such as the Geoscience Laser Altimeter System (GLAS) and the Cloud-Aerosol Lidar and Infrared Pathfinder Satellite Observation (CALIPSO), have provided measurements of the aerosol vertical profiles; however, data coverage is limited due to their narrow footprint and on track pattern (Chaudhry et al., 2007).
5 Although conventional satellite radiometers (e.g. MODIS) have provided aerosol data over the globe scale, only column integrated dust properties in terms of optical thickness have been retrieved (Chu et al., 2002; Kahn et al., 2005). The production of the dust AOD requires a large array of assumptions and approximations (Wielicki et al., 1996). By integrating the available dust information from the preceding observations
10 and constraints into an evolving three-dimensional picture, aerosol transport models can provide a complementary approach to evaluate aerosol radiative forcing (Meloni et al., 2005; Miller et al., 2006).

Most of the general circulation models and RTMs simply assume a prescribed vertical weighting profile based on “climatology” that does not vary in space and time
15 (Haywood et al., 1999; Gu et al., 2006; McComiskey et al., 2008). However, dust vertical distributions can be modified by numerous dynamical processes and can be quite different over dust source regions and downwind areas as documented by a number of previous studies (e.g. Karyampudi et al., 1999; Su and Toon, 2011). GEOS-Chem is a global 3-D CTM, which has been employed to simulate instantaneous AOD with
20 explicit vertical distributions based on aerosol concentrations and optical properties (Tegen and Lacis, 1996). The GEOS-Chem dust simulation is able to capture the seasonal cycle of dust over the Northeast Pacific and the timing and the vertical structure of dust outflow in the free troposphere from Asia during the spring 2001 TRACE-P and ACE-Asia aircraft missions (Fairlie et al., 2007). The present study is motivated by
25 examining the uncertainties of assuming a “climatological” dust vertical profile versus using a more realistic 3-D dust vertical profile simulated by GEOS-Chem to improve our understanding and estimation of global dust radiative forcing and heating rates.

In this study, the global 3-D GEOS-Chem CTM with improved dust emission algorithms is coupled with the Fu-Liou-Gu RTM (Gu et al., 2010, 2011) to examine the

[Title Page](#)[Abstract](#)[Introduction](#)[Conclusions](#)[References](#)[Tables](#)[Figures](#)[|◀](#)[▶|](#)[◀](#)[▶](#)[Back](#)[Close](#)[Full Screen / Esc](#)[Printer-friendly Version](#)[Interactive Discussion](#)

instantaneous dust relative forcing in April 2006. A description of the models and their coupling is presented in Sect. 2, followed by a discussion of the results of the impacts of different dust vertical profiles on the calculations of heating rate and radiative forcing in Sect. 3. A summary and conclusions are given in Sect. 4.

5 2 Model description

2.1 GEOS-Chem

GEOS-Chem is a global 3-D CTM driven by assimilated meteorological observations from the Goddard Earth Observing System (GEOS) of the NASA Global Modeling and Assimilation Office (GMAO) (Bey et al., 2001). We use GEOS-Chem version 8-10 01-04 (<http://acmg.seas.harvard.edu/geos/>) driven by GEOS-5 meteorological fields with 6-h temporal resolution (3-h for surface variables and mixing depths), 2° (latitude) $\times 2.5^\circ$ (longitude) horizontal resolution, and 47 vertical layers between the surface and 0.01 hPa. The GEOS-Chem model includes a fully coupled treatment of tropospheric ozone-NO_x-VOC chemistry and sulfate, nitrate, ammonium, organic carbon (OC), black carbon (BC), mineral dust, and sea salt aerosols (Park et al., 2003, 2004; Alexander et al., 2005; Fairlie et al., 2007). The aerosol optical depth at 550 nm is calculated online assuming lognormal size distributions of externally mixed aerosols and is a function of the local relative humidity to account for hygroscopic growth (Martin et al., 2003). Aerosol optical properties employed here are based on the Global Aerosol Data Set (GADS) (Kopke et al., 1997) with modifications to the size distribution based on field observations (Drury et al., 2010; Jaegle et al., 2011). The wet deposition scheme in GEOS-Chem is described by Liu et al. (2001) for water-soluble aerosols, which includes scavenging in convective updrafts and rainout and washout from large-scale precipitation and convective anvils. Dry deposition is based on the resistance-in-series scheme of Wesely (1990) as implemented by Wang et al. (1998).

Improved estimate of global dust radiative forcing

L. Zhang et al.

Title Page	
Abstract	Introduction
Conclusions	References
Tables	Figures
◀◀	▶▶
◀	▶
Back	Close
Full Screen / Esc	
Printer-friendly Version	
Interactive Discussion	



Improved estimate of global dust radiative forcing

L. Zhang et al.

Title Page	
Abstract	Introduction
Conclusions	References
Tables	Figures
	
	
Back	Close
Full Screen / Esc	
Printer-friendly Version	
Interactive Discussion	

Dust in GEOS-Chem model is distributed in 4 size bins (radii 0.1–1.0, 1.0–1.8, 1.8–3.0, and 3.0–6.0 μm), following Ginoux et al. (2004). The smallest size bin is further divided equally into four sub-micron size bins (with effective radii centered at 0.15, 0.25, 0.4 and 0.8 μm) for determining optical properties and heterogeneous chemistry (Fairlie et al., 2010; Ridley et al., 2012). We use the dust entrainment and deposition (DEAD) mobilization scheme of Zender et al. (2003), combined with the source function used in Global Ozone Chemistry Aerosol Radiation and Transport (GOCART) model (Ginoux et al., 2001; Chin et al., 2004), as described by Fairlie et al. (2007). GEOS-Chem simulates the three-dimensional dust AOD with explicit vertical distributions (Tegen and Lacis, 1996). The optical properties for mineral dust used for the standard GEOS-Chem simulation are based on the refractive indices of Patterson et al. (1977). There is growing recognition that the imaginary component of the refractive index may be too high at UV wavelengths (Colarco et al., 2002). A Mie algorithm (de Rooij and van der Stap, 1984; Mishchenko et al., 1999) is instead used to calculate the optical properties of mineral dust based on the refractive indices of Sinyuk et al. (2003); the single scattering albedo of mineral dust at 300 nm increases by 0.14 to the range of 0.7–0.9 using these new refractive indices (Lee et al., 2009).

Li et al. (2013) improved the dust simulation in GEOS-Chem by using MISR AOD to constrain the global dust emissions, which provides a better simulations of daily surface dust concentration compared to the Interagency Monitoring of Protected Visual Environments (IMPROVE) observations over western US during spring (March–May) 2006. Figure 1a shows global dust emission for April 2006 by applying MISR AOD to constrain the global dust emissions. The simulated global dust emission for April 2006 is 92 Tg, compared to 162 Tg before adjustment. Figure 1b illustrates the vertically integrated column value of simulated dust total AOD for April 2006. High AOD values are located not only over the dust source regions but also over the surrounding downwind areas, which reflect the impact of transport. The vertical structure of the simulated dust AOD will be discussed below.



2.2 Fu–Liou–Gu radiative transfer model

The atmospheric radiative transfer calculations are performed using the Fu–Liou–Gu (FLG) radiative transfer model (RTM), which is a modified and improved version based on the original Fu-Liou scheme (Fu and Liou, 1992, 1993; Gu et al., 2003, 2006, 2010,

- 5 2011). A combination of the delta-four-stream approximation for solar flux calculations (Liou et al., 1988) and delta-two/four-stream approximation for Infrared (IR) flux calculations (Fu et al., 1997) is employed in the model to assure both accuracy and efficiency.

The incorporation of non-gray gaseous absorption in multiple-scattering atmospheres is based on the correlated k-distribution method developed by Fu and Liou (1992).

- 10 Parameterization of the single-scattering properties for cloud particles is implemented by following the procedure developed by Fu and Liou (1993). To increase computational accuracy, the similarity principle for radiative transfer is applied to each grid point to account for the fractional energy in the diffraction peak of the phase function. The solar (0–5 µm) and IR (5–50 µm) spectra are divided into 6 and 12 bands, respectively

- 15 according to the location of prominent atmospheric absorption bands. In the solar spectrum, absorption due to water vapor, O₃, CO₂, O₂, and other minor gases, such as CO, CH₄, and N₂O, is taken into account. Absorption due to water vapor, O₃, CO₂, CH₄, N₂O and CFCs is also considered in the IR spectrum.

- In the radiation scheme, a total of 18 aerosol types have been parameterized by employing the Optical Properties of Aerosols and Clouds (OPAC) database (d'Almeida et al., 1991; Tegen and Lacis, 1996; Hess et al., 1998), which provides the single scattering properties for spherical aerosols computed from the Lorenz–Mie theory in which humidity effects are accounted for. The single scattering properties of the 18 aerosol types for 60 wavelengths in the spectral region between 0.3 µm and 40 µm are interpolated into the 18 FuLiou (Fu and Liou, 1992) spectral bands of the current radiation scheme (Gu et al., 2006). Aerosol types include maritime, continental, urban, five different sizes of mineral dust, insoluble, water soluble, soot (BC), sea salt in two modes

[Title Page](#)

[Abstract](#)

[Introduction](#)

[Conclusions](#)

[References](#)

[Tables](#)

[Figures](#)

◀

▶

◀

▶

[Back](#)

[Close](#)

[Full Screen / Esc](#)

[Printer-friendly Version](#)

[Interactive Discussion](#)



Improved estimate of global dust radiative forcing

L. Zhang et al.

[Title Page](#)[Abstract](#)[Introduction](#)[Conclusions](#)[References](#)[Tables](#)[Figures](#)[◀](#)[▶](#)[◀](#)[▶](#)[Back](#)[Close](#)[Full Screen / Esc](#)[Printer-friendly Version](#)[Interactive Discussion](#)

(accumulation mode and coarse mode), mineral dust in four different modes (nucleation mode, accumulation mode, coarse mode, and transported mode), and sulfate droplets.

In the current FLG-RTM, the input AOD represents the vertically integrated column value, which has been distributed vertically according to a certain weighting profile based on the layer pressure and scale height (height at which the aerosol loading is reduced to e^{-1} of the surface value) (Gu et al., 2006). The aerosol loading decreases exponentially and the highest aerosol layer in the model are placed at 15 km (Charlock et al., 2004). This represents a set of distributions that can be simply described by an exponential function with different scale heights. Such vertical distributions are typically used by radiative transfer models (e.g. McComiskey et al., 2008) and can be traced back to the work of Elterman (1968).

In this study, the visible surface albedo and the atmospheric vertical profiles of pressure, temperature, water vapor, and O₃ provided by GEOS-Chem meteorological data are used to drive the FLG-RTM. The spatial variations of solar zenith angle and emissivity are not taken into account since the purpose is to assess the sensitivity of radiative forcing to different dust AOD vertical profiles. Thus, the cosine of the solar zenith angle of 0.5 and emissivity of 1 are used in the calculations. The same column-integrated AOD of dust simulated by GEOS-Chem (Fig. 1b) is used as the input to calculate the radiative forcing except for the different vertical profiles. One is based on the default vertical weighting profile in FLG as mentioned above. The other is according to the simulated dust vertical distribution in GEOS-Chem. The present study will focus on the instantaneous monthly mean results of April 2006.

3 Vertical structure of dust AOD by using different vertical profile

Figure 1 illustrates the dust sources over the world, which shows two major dust regions over Africa and Asia. North Africa is a major source region for desert dust during the spring season (Prospero et al., 2002), with nearly 700 Tg of dust aerosols produced annually in the Saharan desert (Laurent et al., 2008). The African and Asian deserts

Improved estimate of global dust radiative forcing

L. Zhang et al.

[Title Page](#)[Abstract](#)[Introduction](#)[Conclusions](#)[References](#)[Tables](#)[Figures](#)[◀](#)[▶](#)[◀](#)[▶](#)[Back](#)[Close](#)[Full Screen / Esc](#)[Printer-friendly Version](#)[Interactive Discussion](#)

Improved estimate of global dust radiative forcing

L. Zhang et al.

there is another widespread high AOD in the middle troposphere over a broad swath from 5° W to 60° E over the southern Europe, which reflects the impact of transport of dust from the African source region. The maximum AOD over the Asian source region is much lower than that of the African source region. For the non-dust source regions, the maximum AOD is found in the middle troposphere over the downwind areas of African and Asian dust belts.

The altitude-longitude cross-sections of dust AOD, averaged over African and Asian dust belts using the FLG vertical profile, are shown in Fig. 3. Different from that in the GEOS-Chem vertical profile, the maximum AOD is close to the surface. It consistently decreases with increasing altitude globally, including both the dust and non-dust source regions. The deficiency is evident by using such prescribed “climatological” vertical profile since the non-dust source regions and ocean areas have the same vertical profiles as those of the dust source regions with the maximum AOD at the surface.

The differences in dust AOD vertical distributions, using the same column-integrated AOD as shown in Fig. 1b, between using GEOS-Chem or FLG vertical profile over the African and Asian dust belts are shown in Fig. 4. Using the GEOS-Chem vertical profile for the African dust belt produces much higher AOD in the middle troposphere (800–550 hPa); up to a factor of 2 higher than from using the FLG vertical profile. Lower values of AOD are found in the low troposphere (1000–800 hPa) and above 550 hPa over the North African areas (20° W– 40° E). The positive differences of AOD are shown in the middle to upper troposphere over areas downwind of the African dust belt. This suggests that more dust particles might be lifted into the free troposphere using the GEOS-Chem vertical profile (Fig. 4a). These differences are more significant over the Asian dust belt (Fig. 4b). The values of AOD are increased by a factor of 5 in the middle to upper troposphere using GEOS-Chem vertical profile over the Asian dust source region and downwind areas. Similarly, the dust AOD averaged over the Asian dust belt is much lower near the surface layer (1000–800 hPa) with the GEOS-Chem vertical profile. Obviously, the impact of transport of dust is not reflected by using FLG

Title Page	
Abstract	Introduction
Conclusions	References
Tables	Figures
◀	▶
◀	▶
Back	Close
Full Screen / Esc	
Printer-friendly Version	
Interactive Discussion	



Improved estimate of global dust radiative forcing

L. Zhang et al.

[Title Page](#)[Abstract](#)[Introduction](#)[Conclusions](#)[References](#)[Tables](#)[Figures](#)[◀](#)[▶](#)[◀](#)[▶](#)[Back](#)[Close](#)[Full Screen / Esc](#)[Printer-friendly Version](#)[Interactive Discussion](#)

vertical profile, which results in significant differences compared to the GEOS-Chem vertical profile along downwind areas of source regions.

The simulated total AOD of dust is the sum of the AOD of each size bin, and is dominated by the first three small size bins. The smallest ($0.7\text{ }\mu\text{m}$) dust particles play important roles in contributing to the large values of AOD over the African and Asian dust source regions primarily due to large particles in the coarse mode being removed from the distribution from gravitational settling. The differences of dust AOD between using GEOS-Chem vertical profile and FLG vertical profile for each size bins are shown in Fig. 5. Their differences are similar to that of the total dust AOD, with much higher AOD in the middle troposphere while lower at the surface using the GEOS-Chem vertical profile. Meanwhile, the differences between GEOS-Chem vertical profile and FLG vertical profile for the smallest size bin ($0.7\text{ }\mu\text{m}$) are most significant, and contribute more than 70 % to the differences of total dust AOD over the dust source regions (see Fig. 5a). It suggests that more small dust particles are lifted to the middle and upper troposphere, especially over the downwind areas. The clay aerosols (diameter $< 2\text{ }\mu\text{m}$) have lifetimes on the order of a week and produce a strong negative radiative forcing by efficiently scattering shortwave radiation (Kok, 2011). On the other hand, the clear sky thermal IR radiative forcing and cloudy sky TOA solar radiative forcing of dust aerosols are very sensitive to the altitude of the dust and cloud layers (Liao and Seinfeld, 1998). Therefore, the vertical differences of AOD produced by small dust particles would undoubtedly result in significant impacts on radiation and heating.

4 Impact of vertical profiles on radiative forcing

The net radiative forcing, ΔF , of solar and IR radiation has been calculated as the change of the net radiation (downward flux, F_{down} , minus upward flux, F_{up}) at the top of atmosphere and at the surface when the dust aerosols are present with respect to the



Improved estimate of global dust radiative forcing

L. Zhang et al.

[Title Page](#)

[Abstract](#)

[Introduction](#)

[Conclusions](#)

[References](#)

[Tables](#)

[Figures](#)

[◀](#)

[▶](#)

[◀](#)

[▶](#)

[Back](#)

[Close](#)

[Full Screen / Esc](#)

[Printer-friendly Version](#)

[Interactive Discussion](#)



clear air (no dust aerosol) case, according to:

$$\Delta F = F_{\text{down}} - F_{\text{up}} \quad (1)$$

$$\text{RF} = \Delta F_{\text{aerosol}} - \Delta F_{\text{clear}} \quad (2)$$

- 5 The daily changes of the AOD and of the aerosol optical properties are not taken into account since the purpose is to assess the sensitivity of the direct radiative forcing influenced by differences in dust AOD vertical profiles. To examine the radiative forcing in different regions, we focus our analysis on the source regions of Sahara desert (10° N– 25° N, 10° W– 40° E) and Gobi desert (40° N– 45° N, 90° E– 110° E), as well as their downwind areas of Arabian Sea (5° N– 25° N, 60° E– 75° E) and Eastern Asian (35° N– 55° N, 120° E– 150° E).

4.1 Impact of vertical profiles on solar radiative forcing

- Table 1 shows the solar and IR radiative forcing at the TOA and at the surface. The solar radiative forcing at the TOA depends on the surface albedo and properties of the atmospheric column as well as the dust optical properties. Generally, the solar radiative forcing at the TOA is negative for maritime, sulfate and small mineral dust particles, which scatter solar radiation with little absorption produced (Gu et al., 2006). Dust particles increase the apparent reflectance of the earth over dark surfaces (e.g. ocean); more solar radiation is scattered back to space in the presence of slightly absorbing aerosol. The model predicts a negative solar radiative forcing and exerts cooling effect at the TOA throughout entire atmosphere except with some bright surfaces for both vertical profiles (Fig. 6a, b). The absorption of solar radiation dominates over scattering over bright surfaces (such as snow covered areas), or cloud-covered surfaces, causing a net TOA warming (Weaver et al., 2002). Therefore, the positive values of $0 \sim 1$ are shown over the snow areas in high latitude. The positive solar radiative forcing over part of the desert is due to the elevated absorbing dust particles above the highly reflective desert surface (Huang et al., 2009). The solar radiative forcing over both dust source

regions and downwind areas exerts significant cooling effect at the TOA. The global mean values of solar radiative forcing at the TOA are -1.85 and -1.73 , respectively for the GEOS-Chem vertical profile and FLG vertical profile. The difference in the solar radiative forcing at the TOA between the GEOS-Chem vertical profile and the FLG vertical profile (the former minus later) is shown in Fig. 6c. With the GEOS-Chem vertical profile, the cooling effect is weaker by 0.19 W m^{-2} and 0.24 W m^{-2} over the Sahara and Gobi deserts than that with FLG vertical profile. The FLG vertical profile allows for more dust particles in the upper troposphere over the dust source regions than that of the GEOS-Chem vertical profile (Figs. 3 and 5), which exerts more cooling at the TOA. However, more dust particles, especially the small size particles that mostly scatter solar radiation, are lifted into the middle and upper troposphere over the downwind areas by using the GEOS-Chem vertical profile (Figs. 4 and 5). This results in more reflection at the TOA and much stronger cooling effect over all except Arabian Sea, which shows weaker cooling. A possible reason for is that Arabian Sea is located close to the dust source regions of Sahara desert and Arabian Peninsula. Other than some far away downwind areas (e.g. Eastern Asian), the vertical structure of dust distribution over Arabian Sea follows that of the African source region (Fig. 2), leading to similar radiative impact (Table 1). The solar radiative forcing is less dependent on the vertical profile for low absorbing particles at the TOA than that of absorbing particles, with up to a 10 % variation in the daily average forcing over the dust source region (Meloni et al., 2005). Here, the differences in averaged solar radiative forcing at the TOA between using GEOS-Chem vertical profile and FLG vertical profile are less than 3 % over the Sahara and Gobi desert. However, the impact of the vertical profile on the solar radiative forcing over the downwind areas is much larger than that over the dust source region. The differences are about 10 % over Arabian Sea and Eastern Asia.

Even though the TOA forcing is often small, the surface forcing can be relatively large, especially over the dust source regions. Both solar absorption and reflection within the atmosphere tend to cool the surface (Fig. 7). The solar radiative forcing at the surface is negative (cooling effect) with a global mean value of -3.42 W m^{-2} for

Improved estimate of global dust radiative forcing

L. Zhang et al.

Title Page	
Abstract	Introduction
Conclusions	References
Tables	Figures
	
	
Back	Close
Full Screen / Esc	
Printer-friendly Version	
Interactive Discussion	



Improved estimate of global dust radiative forcing

L. Zhang et al.

GEOS-Chem vertical profile and -3.46 W m^{-2} for FLG vertical profile (Table 1). It increases significantly to more than -20 W m^{-2} over the dust source regions of Sahara and Gobi deserts, indicating a decrease in the solar insolation at the surface associated with more scattering and absorption of radiation by dust particles. The differences of solar radiative forcing at the surface between GEOS-Chem vertical profile and FLG vertical profile are evident over the dust source regions and their surrounding downwind areas, such as Arabian Sea (Fig. 7c). With the GEOS-Chem vertical profile, less cooling is produced over the Sahara, Gobi and Arabian Sea than that with FLG vertical profile (Table 1).

10 4.2 Differences of solar radiative forcing over dust source regions and downwind areas

In order to explain the differences in the dust radiative forcing between the dust source regions and downwind areas, two samples were selected from the dust source region of Sahara desert ($10^\circ \text{ E}, 20^\circ \text{ N}$) and downwind areas of Eastern Asia ($140^\circ \text{ E}, 40^\circ \text{ N}$)

15 to show the impact of different AOD vertical structures on the radiative forcing through the atmosphere (see Figs. 8 and 9). At the TOA, the differences of net radiative forcing between GEOS-Chem vertical profile and FLG vertical profile are dominated by the differences of the upward flux since the downward flux is the same at the TOA. The differences in the upward flux at the TOA are positively correlated to the differences of AOD in the upper troposphere where less dust particles over the source regions lead to less solar reflection and less upward flux for low absorbing aerosols. Thus, differences in net forcing between the GEOS-Chem vertical profile and the FLG vertical profile at the TOA are found to be positive over the dust source regions (Fig. 8b) and negative over the downwind areas (Fig. 9b). Vertically, the change of downward flux 20 at a certain layer is negatively correlated to the change of AOD in that layer. Fewer particles lead to less reflection and absorption, resulting in more downward flux at the bottom of that layer. The change of upward flux is normally proportional to the

25



Title Page	
Abstract	Introduction
Conclusions	References
Tables	Figures
	
	
Back	Close
Full Screen / Esc	
Printer-friendly Version	
Interactive Discussion	

Title Page	
Abstract	Introduction
Conclusions	References
Tables	Figures
	
	
Back	Close
Full Screen / Esc	
Printer-friendly Version	
Interactive Discussion	

change of downward flux, where more downward flux leads to more upward flux. When the vertical change of AOD is positive/negative, the corresponding differences in net flux will be decreasing/increasing. Less AOD above 600 hPa with GEOS-Chem vertical profile over the dust source region (Fig. 8a) leads to an increasing downward flux from TOA to 600 hPa (Fig. 8b). Therefore, the differences of net radiative forcing between GEOS-Chem vertical profile and FLG vertical profile exert an increasing trend. More dust particles are seen at 600–800 hPa by using the GEOS-Chem vertical profile, which increases both scattering and absorption of solar radiation, leading to a decreasing trend for downward flux at 700–800 hPa due to the reduction of available radiation. The positive differences in net radiative forcing are due the magnitude of the much larger differences in downward flux. Over the downwind areas, though the dust AOD vertical profiles are quite different to those over source region, results are similarly concluded that the differences of net radiative forcing between GEOS-Chem vertical profile and FLG vertical profile show decreasing and negative values above 700 hPa (Fig. 9b) due to the much larger AOD using the GEOS-Chem vertical profile in that vertical region (Fig. 9a). The impact of vertical profiles on solar radiative forcing at the surface is more complicated relative to that at the TOA since it depends on not only the available downward radiation throughout the atmospheric column, but also the upward flux at the surface.

4.3 Impact of vertical profiles on IR radiative forcing

In addition to the solar radiative forcing, as one of the absorbing aerosols, dust particles also exert a significant thermal IR radiative forcing, thus contributing to the greenhouse effect (Haywood et al., 2005; Gu et al., 2006; Shell et al., 2007). The definition of IR radiative forcing is similar to that of the solar radiative forcing, the difference between irradiances with and without aerosol at the TOA and surface. Unlike the solar radiative forcing which is a strong function of the solar zenith angle (Meloni et al., 2005), the IR radiative forcing is effective for the full 24 h and is a strong function of the surface temperature (Haywood et al., 2005). Dust particles have a warming effect at the TOA



Improved estimate of global dust radiative forcing

L. Zhang et al.

[Title Page](#)[Abstract](#)[Introduction](#)[Conclusions](#)[References](#)[Tables](#)[Figures](#)[◀](#)[▶](#)[◀](#)[▶](#)[Back](#)[Close](#)[Full Screen / Esc](#)[Printer-friendly Version](#)[Interactive Discussion](#)

in IR radiation for both GEOS-Chem vertical profile and FLG vertical profile over the African and Asian dust source regions and their downwind areas (Fig. 10). The average IR radiative forcing over the Saharan desert is about 1.6 W m^{-2} and 1.8 W m^{-2} at the TOA for GEOS-Chem vertical profile and FLG vertical profile, respectively. This warming effect at the TOA is also dependent on the size of the dust particles (Gu et al., 2006). The IR radiation interacts more efficiently with larger particles, while the solar radiation interacts more efficiently with smaller particles (Yoshioka et al., 2007). Therefore, the IR forcing is highest near dust source regions where more large dust particles are present since larger particles have shorter lifetimes and travel shorter distances (Kok et al., 2011).

The differences of IR forcing between the GEOS-Chem vertical profile and the FLG vertical profile at the TOA are apparent. Since there are less large dust particles in the middle and upper troposphere by using the GEOS-Chem vertical profile, the IR forcing is lower by 0.17 W m^{-2} and 0.14 W m^{-2} by using GEOS-Chem vertical profile than that by using FLG vertical profile over both Saharan desert and the Arabian Sea (Fig. 10c). However, the warming effect with GEOS-Chem vertical profile is 0.44 W m^{-2} and 0.06 W m^{-2} higher than that of FLG vertical profile over the downwind area of Eastern Asia due to more dust particles in the free troposphere (see Figs. 3 and 5). At the surface, the IR forcing is smaller than the solar forcing over the dust source regions (Fig. 11). Dust absorption reduces the reemission at the top of the atmosphere and increases the downward irradiance at the surface, leading to a positive IR radiative forcing and warming at the surface. The warming effect of IR radiation is much smaller globally by using the GEOS-Chem vertical profile at the surface.

While an increased IR warming (due to the dust “greenhouse effect”) somewhat balances the cooling, the net result is typically negative (Shell et al., 2007). The global average net forcing is dominated by the solar forcing with a cooling effect at the TOA and at the surface for both the GEOS-Chem vertical profile and the FLG vertical profile. The net cooling is about -17.0 W m^{-2} over the Sahara desert and -22.0 W m^{-2} over the Gobi desert by using the GEOS-Chem vertical profile. The net forcing at the surface

over Eastern Asia is -10.6 W m^{-2} with the GEOS-Chem vertical profile, which exerts more significant cooling than that of using FLG vertical profile.

5 Impact of vertical profiles on heating rate

Dust particles not only scatter but also absorb solar and IR radiation, which can influence the heating profiles and contribute to large diabatic heating in the atmosphere (Fu et al., 1997; Huang et al., 2006). Model studies show that an elevated Saharan dust layer can change the atmospheric heating rate significantly (Carlson and Benjamin, 1980). The GEOS-Chem coupled FLG-RTM is also used to calculate the solar and IR dust heating rate based on GEOS-Chem vertical profile and FLG vertical profile in this study.

Figures 12–14 show the impact of dust particles on the solar, IR, and net heating rates over the two dust belts by using GEOS-Chem vertical profile and FLG vertical profile, respectively. They are calculated as the differences between the simulated radiative heating rates with and without the dust particles. The pattern of solar heating rate is consistent with that of the dust AOD due to the absorption of solar radiation by dust. Dust particles heat the atmosphere by more than 0.5 K day^{-1} over African and Asian source regions for both GEOS-Chem vertical profile and FLG vertical profile (Fig. 12a, b), but there is slight cooling effect near the surface over the non-dust source regions by using GEOS-Chem vertical profile. The solar heating rate shows a maximum corresponding to that of the high dust AOD. The differences of the heating rates between GEOS-Chem vertical profile and FLG vertical profile (Fig. 12c) are consistent with the differences of their AOD distribution (Fig. 4). The maximum of the difference is shown at 700 hPa over the African dust source region. Although dust particles exert less effect on IR radiative heating rates with very small values (Fig. 13), they do show a warming effect near surface over the non-dust source regions while significant cooling effect in the low and middle troposphere over the dust source regions. The IR cooling ranges from 0.06 K day^{-1} to 0.08 K day^{-1} , which partly compensates the large

[Title Page](#)

[Abstract](#)

[Introduction](#)

[Conclusions](#)

[References](#)

[Tables](#)

[Figures](#)

◀

▶

◀

▶

[Back](#)

[Close](#)

[Full Screen / Esc](#)

[Printer-friendly Version](#)

[Interactive Discussion](#)



solar radiative heating near the dust layers. Fig. 14 shows the net heating by using the GEOS-Chem and the FLG vertical profiles over the two dust belts. The vertical distribution of net radiative heating is similar to that of the dust AOD. The maximum radiative net heating rate is consistent with the highest AOD distribution. The net dust heating at the dust layer is about 0.2 K day^{-1} to 0.5 K day^{-1} over the dust source regions for both vertical profiles. The dust radiative net heating based on GEOS-Chem vertical profile reflects the impact of transport. The net heating rate due to the dust particles are less than 0.05 K day^{-1} above the dust layer and the non-dust source regions. The differences of the net heating rate between GEOS-Chem vertical profile and FLG vertical profile are the same as those of the solar heating rate (Figs. 12c and 14c) since the net heating rate is dominated by the solar heating rate (Huang et al., 2009). An enhanced net heating rate is evident in the middle and upper troposphere over African and Asian source regions by using GEOS-Chem vertical profile, but it is much smaller by 0.1 K day^{-1} near surface layers compare to using FLG vertical profile (Fig. 14c). Obviously, the radiative net heating is sensitive to the dust AOD vertical profile, which may play an important role in modulating regional circulation.

6 Summary and conclusion

We have used the GEOS-Chem global 3-D CTM with improved dust emission coupled with the FLG spectral radiative transfer model to investigate the fluxes of solar and infrared radiation at the TOA and the surface based on the simulated instantaneously GEOS-Chem vertical profile and prescribed “climatological” FLG vertical profile. Using the GEOS-Chem vertical profile reflects the differences of vertical structure of AOD between dust and non-dust source regions, while using FLG vertical profile shows a consistent pattern of AOD vertical structure both in dust and non-dust source regions. The coupled calculations involving GEOS-Chem and FLG-RTM with the GEOS-Chem vertical profile minimizes the physical inconsistencies between the 3-D CTM aerosol fields and the radiative transfer calculations and contribute directly to the evaluation of

[Title Page](#)[Abstract](#)[Introduction](#)[Conclusions](#)[References](#)[Tables](#)[Figures](#)[◀](#)[▶](#)[Back](#)[Close](#)[Full Screen / Esc](#)[Printer-friendly Version](#)[Interactive Discussion](#)

dust heating rate and radiative forcing. The dust AOD is consistently high from surface to 600 hPa over the African and Asian dust source regions; then it decreases with increasing altitude when using the GEOS-Chem vertical profile. The largest AOD is in the middle troposphere second only to the surface for non-dust source regions (along the 5 downwind areas). The largest solar heating rate is consistent with the maximum of dust AOD due to the absorption by dust particles. The radiative net heating dominated by the solar heating rate is also sensitive to different vertical profiles and shows substantial differences between the GEOS-Chem vertical profile and the FLG vertical profile. The net heating rate is much larger in the middle and upper troposphere over the African 10 and Asian source regions, while smaller near surface layers when using GEOS-Chem vertical profile. Differences due to dust vertical profiles could play an important role in modulating regional circulation.

The global mean radiative forcing is negative in the solar part of the spectrum, associated with the predominantly scattering nature of dust particles at these wavelengths, 15 while positive in the thermal infrared. The vertical distributions of dust particles strongly affect the estimated radiative forcing at TOA and the surface. With GEOS-Chem vertical profile, dust particles have negative radiative forcings at both TOA and the surface with globally averaged values of about -1.85 W m^{-2} and -3.42 W m^{-2} , respectively. This reduces solar radiative forcing by about $0.2\text{--}0.25 \text{ W m}^{-2}$, but also increases IR 20 radiative forcing by about $0.1\text{--}0.2 \text{ W m}^{-2}$ at the TOA over the African and Asia dust source regions. Additionally, we saw a reduction of 1.0 W m^{-2} in solar radiative forcing and an increase of 0.4 W m^{-2} in IR radiative forcing at TOA over the downwind areas in Eastern Asia by using GEOS-Chem vertical profile, as compared to FLG vertical profile.

25 The dust radiative forcing is negative in the solar spectrum, while positive in the thermal infrared at the surface for both the GEOS-Chem vertical profile and the FLG vertical profile. With GEOS-Chem vertical profile, the global average is -3.4 W m^{-2} in solar radiation and 0.4 W m^{-2} in thermal IR radiation. The net radiation is 3 W m^{-2} at the surface, which is the same as in the case of FLG vertical profile. However, the radiative

[Title Page](#)[Abstract](#)[Introduction](#)[Conclusions](#)[References](#)[Tables](#)[Figures](#)[Back](#)[Close](#)[Full Screen / Esc](#)[Printer-friendly Version](#)[Interactive Discussion](#)

forcing effect of dust particles is more significant by using FLG vertical profile at the surface over Eastern Asia, while less significant over Sahara and Gobi deserts. The decrease (increase) of net radiative forcing at the surface accompanied by increased (decreased) atmospheric heating rate can be a significant forcing of regional circulation and convection.

References

- Alexander, B., Savarino, J., Lee, C. C. W., Park, R. J., Jacob, D. J., Thiemens, M. H., Li, Q. B., and Yantosca, R. M.: Sulfate formation in sea-salt aerosols: constraints from oxygen isotopes, *J. Geophys. Res.*, 110, D10307, doi:10.1029/2004JD005659, 2005.
- 10 Andreae, M. O.: Climatic effects of changing atmospheric aerosol levels, in: Future Climates of the World: a Modelling Perspective, World Survey of Climatology, Vol. 16, edited by: Henderson-Sellers, A., Elsevier, New York, 347–398, 1995.
- Bey, I., Jacob, D. J., Yantosca, R. M., Logan, J. A., Field, B. D., Fiore, A. M., Li, Q. B., Liu, H. G. Y., Mickley, L. J., and Schultz, M. G.: Global modeling of tropospheric chemistry with assimilated meteorology: model description and evaluation, *J. Geophys. Res.*, 106, 23073–23096, 2001.
- 15 Carlson, T. N. and Benjamin, S. G.: Radiative heating rates for Saharan dust, *J. Atmos. Sci.*, 37, 193–213, 1980.
- Charlock, T. P., Rose, F. G., Rutan, D., Jin, Z., Fillmore, D., and Collins, W.: Global retrieval of the surface and atmospheric radiation budget and direct aerosol forcing, paper presented at Conference on Satellite Meteorology, p. 8.11, Am. Meteorol. Soc., Norfolk, VA, 2004.
- 20 Chaudhry, Z., Martins, J. V., Li, Z., Tsay, S.-C., Chen, H., Wang, P., Wen, T., Li, C., and Dickerson, R. R.: In situ measurements of aerosol mass concentration and radiative properties in Xianghe, southeast of Beijing, *J. Geophys. Res.*, 112, D23S90, doi:10.1029/2007JD009055, 2007.
- 25 Chin, M., Chu, A., Levy, R., Remer, L., Kaufman, Y., Holben, B., Eck, T., Ginoux, P., and Gao, Q.: Aerosol distribution in the Northern Hemisphere during ACE-Asia: results from global model, satellite observations, and Sun photometer measurements, *J. Geophys. Res.*, 109, D23S90, doi:10.1029/2004JD004829, 2004.

Title Page	
Abstract	Introduction
Conclusions	References
Tables	Figures
	
	
Back	Close
Full Screen / Esc	
Printer-friendly Version	
Interactive Discussion	



- Chu, D. A., Kaufman, Y. J., Ichoku, C., Remer, L. A., Tanre, D., and Holben, B. N.: Validation of MODIS aerosol optical depth retrieval over land, *Geophys. Res. Lett.*, 29, 8007, doi:10.1029/2001GL013205, 2002.
- Colarco, P. R., Toon, O. B., Torres, O., and Rasch, F. J.: Determining the UV imaginary part of refractive index of Saharan dust particles from TOMS data and a three dimensional model of dust transport, *J. Geophys. Res.*, 107, 4289, doi:10.1029/2001JD000903, 2002.
- d'Almeida, G. A., Koepke, P., and Shettle, E. P.: Atmospheric Aerosols – Global Climatology and Radiative Characteristics, A. Deepak, Hampton, Va, 561 pp., 1991.
- de Rooij, W. A. and van der Stap, C. C. A. H.: Expansion of Mie scattering matrices in generalized spherical functions, *Astron. Astrophys.*, 131, 237–248, 1984.
- Drury, E., Jacob, D. J., Spurr, R. J. D., Wang, J., Shinozuka, Y., Anderson, B. E., Clarke, A. D., Dibb, J., McNaughton, C., and Weber, R.: Synthesis of satellite (MODIS), aircraft (ICARTT), and surface (IMPROVE, EPA-AQS, AERONET) aerosol observations over eastern North America to improve MODIS aerosol retrievals and constrain surface aerosol concentrations and sources, *J. Geophys. Res.*, 115, D14204, doi:10.1029/2009JD012629, 2010.
- Elterman, L.: UV, Visible and IR Attenuation for Altitudes to 50 km, Rep. AFCR-68-0153, Air Force Cambridge Res. Lab., Bedford, Mass, 1968.
- Fairlie, T. D., Jacob, D. J., and Park, R. J.: The impact of transpacific transport of mineral dust in the United States, *Atmos. Environ.*, 41, 1251–1266, 2007.
- Fairlie, T. D., Jacob, D. J., Dibb, J. E., Alexander, B., Avery, M. A., van Donkelaar, A., and Zhang, L.: Impact of mineral dust on nitrate, sulfate, and ozone in transpacific Asian pollution plumes, *Atmos. Chem. Phys.*, 10, 3999–4012, doi:10.5194/acp-10-3999-2010, 2010.
- Fu, Q. and Liou K. N.: On the correlated k-distribution method for radiative transfer in nonhomogeneous atmospheres, *J. Atmos. Sci.*, 49, 2139–2156, 1992.
- Fu, Q. and Liou K. N.: Parameterization of the radiative properties of cirrus clouds, *J. Atmos. Sci.*, 50, 2008–2025, 1993.
- Fu, Q., Liou, K. N., Cribb, M. C., Charlock, T. P., and Grossman, A.: Multiple scattering parameterization in thermal infrared radiative transfer, *J. Atmos. Sci.*, 54, 2799–2812, 1997.
- Gadhavi, H. and Jayaraman, A.: Airborne lidar study of the vertical distribution of aerosol over Hyderabad, an urban site in central India, and its implication for radiative forcing calculations, *Ann. Geophys.*, 24, 2461–2470, 2006,
<http://www.ann-geophys.net/24/2461/2006/>.

Improved estimate of global dust radiative forcing

L. Zhang et al.

[Title Page](#)[Abstract](#)[Introduction](#)[Conclusions](#)[References](#)[Tables](#)[Figures](#)[Back](#)[Close](#)[Full Screen / Esc](#)[Printer-friendly Version](#)[Interactive Discussion](#)

Improved estimate of global dust radiative forcing

L. Zhang et al.

[Title Page](#)

[Abstract](#)

[Introduction](#)

[Conclusions](#)

[References](#)

[Tables](#)

[Figures](#)

[◀](#)

[▶](#)

[◀](#)

[▶](#)

[Back](#)

[Close](#)

[Full Screen / Esc](#)

[Printer-friendly Version](#)

[Interactive Discussion](#)



Ginoux, P., Chin, M., Tegen, I., Prospero, J. M., Holben, B., Dubovik, O., and Lin, S.-J.: Sources and distributions of dust aerosols simulated with the GOCART model, *J. Geophys. Res.*, 106, 20255–20274, 2001.

Ginoux, P., Prospero, J. M., Torres, O., Chin, M.: Long-term simulation of global dust distribution with the GOCART model: correlation with North Atlantic oscillation, *Environ. Model. Softw.*, 19, 113–128, 2004.

Gu, Y., Farrara, J., Liou, K. N., and Mechoso, C. R.: Parameterization of cloud-radiation processes in the UCLA general circulation model, *J. Climate*, 16, 3357–3370, 2003.

Gu, Y., Liou, K. N., Xue, Y., Mechoso, C. R., Li, W., and Luo, Y.: Climatic effects of different aerosol types in China simulated by the University of California, Los Angeles atmospheric general circulation model, *J. Geophys. Res.*, 111, D15201, doi:10.1029/2005JD006312, 2006.

Gu, Y., Liou, K. N., Chen, W., and Liao, H.: Direct climate effect of black carbon in China and its impact on dust storms, *J. Geophys. Res.*, 115, D00K14, doi:10.1029/2009JD013427, 2010.

Gu, Y., Liou, K. N., Ou, S. C., and Fovell, R.: Cirrus cloud simulations using WRF with improved radiation parameterization and increased vertical resolution, *J. Geophys. Res.*, 116, D06119, doi:10.1029/2010JD014574, 2011.

Hamonou, E., Chazette, P., Balis, D., Dulac, F., Schneider, X., Galani, E., Ancellet, G., and Paayannnis, A.: Characterization of the vertical structure of Saharan dust export to the Mediterranean basin, *J. Geophys. Res.*, 104(D18), 22257–22270, doi:10.1029/1999JD900257, 1999.

Haywood, J. M., Ramaswamy, V., and Soden, B. J.: Tropospheric aerosol climate forcing in clear-sky satellite observations over the oceans, *Science*, 283, 1299–1305, 1999.

Haywood, J. M., Allan, R. P., Culverwell, I., Slingo, T., Milton, S., Edwards, J., and Clerbaux, N.: Can desert dust explain the outgoing longwave radiation anomaly over the Sahara during July 2003?, *J. Geophys. Res.*, 110, D05105, doi:10.1029/2004JD005232, 2005.

Hess, M., Koepke, P., and Schult, I.: Optical properties of aerosols and clouds: the software package OPAC, *B. Am. Meteorol. Soc.*, 79, 831–844, 1998.

Huang, J., Lin, B., Minnis, P., Wang, T., Wang, X., Hu, Y., Yi, Y., and Ayers, J. K.: Satellite-based assessment of possible dust aerosols semidirect effect on cloud water path over East Asia, *Geophys. Res. Lett.*, 33, L19802, doi:10.1029/2006GL026561, 2006.

Huang, J., Fu, Q., Su, J., Tang, Q., Minnis, P., Hu, Y., Yi, Y., and Zhao, Q.: Taklimakan dust aerosol radiative heating derived from CALIPSO observations using the Fu-Liou radiation

model with CERES constraints, *Atmos. Chem. Phys.*, 9, 4011–4021, doi:10.5194/acp-9-4011-2009, 2009.

Huebert, B. J., Howell, S. G., Zhuang, L., Heath, J. A., Litchy, M. R., Wylie, D. J., Kreidler-Moss, J. L., Cöppicus, S., and Pfeiffer, J. E.: Filter and impactor measurements of anions and cations during the First Aerosol Characterization Experiment (ACE 1), *J. Geophys. Res.*, 103, 16493–16509, 1998.

Intergovernmental Panel on Climate Change: The Physical Science Basis. Contribution of Working Group I to the Fourth Assessment Report of the Intergovernmental Panel on Climate Change, edited by: Solomon, S., Qin, D., Manning, M., Chen, Z., Marquis, M., Averyt, K. B., Tignor, M., and Miller, H. L., Cambridge Univ. Press, Cambridge, UK, 2007.

Jaeglé, L., Quinn, P. K., Bates, T. S., Alexander, B., and Lin, J.-T.: Global distribution of sea salt aerosols: new constraints from in situ and remote sensing observations, *Atmos. Chem. Phys.*, 11, 3137–3157, doi:10.5194/acp-11-3137-2011, 2011.

Johnson, B. T., Heese, B., McFarlane, S. A., Chazette, P., Jones, A., and Bellouin, N.: Vertical distribution and radiative effects of mineral dust and biomass burning aerosol over West Africa during DABEX, *J. Geophys. Res.*, 113, D00C12, doi:10.1029/2008JD009848, 2008.

Kahn, R. A., Gaitley, B. J., Martonchik, J. V., Diner, D. J., and Crean, K. A.: Multiangle Imaging Spectroradiometer (MISR) global aerosol optical depth validation based on 2 years of coincident Aerosol Robotic Network (AERONET) observations, *J. Geophys. Res.*, 110, D10S04, doi:10.1029/2004JD004706, 2005.

Karyampudi, V. M., Palm, S. P., Reagen, J. A., Fang, H., Grant, W. B., Hoff, R. M., Moulin, C., Pierce, H. F., Torres, O., Browell, E. V., and Melfi, S. H.: Validation of the Saharan dust plume conceptual model using lidar, Meteosat, and ECMWF data, *B. Am. Meteorol. Soc.*, 80, 1045–1075, 1999.

Kok, J. F.: A scaling theory for the size distribution of emitted dust aerosols suggests climate models underestimate the size of the global dust cycle, *P. Natl. Acad. Sci. USA*, 108, 1016–1021, 2011.

Kopke, P., Hess, M., Schult, I., and Shettle, E. P.: Global Aerosol Data Set Rep., Max 873 Planck Inst. für Meteorol., Hamburg, Germany, 1997.

Laurent, B., Marticorena, B., Bergametti, G., Léon, J. F., and Mahowald, N. M.: Modeling mineral dust emissions from the Sahara desert using new surface properties and soil database, *J. Geophys. Res.*, 113, D14218, doi:10.1029/2007JD009484, 2008.

Improved estimate of global dust radiative forcing

L. Zhang et al.

[Title Page](#)

[Abstract](#)

[Introduction](#)

[Conclusions](#)

[References](#)

[Tables](#)

[Figures](#)

◀

▶

◀

▶

[Back](#)

[Close](#)

[Full Screen / Esc](#)

[Printer-friendly Version](#)

[Interactive Discussion](#)



Improved estimate of global dust radiative forcing

L. Zhang et al.

[Title Page](#)

[Abstract](#)

[Introduction](#)

[Conclusions](#)

[References](#)

[Tables](#)

[Figures](#)

◀

▶

◀

▶

[Back](#)

[Close](#)

[Full Screen / Esc](#)

[Printer-friendly Version](#)

[Interactive Discussion](#)



Improved estimate of
global dust radiative
forcing

L. Zhang et al.

- Miller, R. L., Cakmur, R. V., Perlitz, J., Geogdzhayev, I. V., Ginoux, P., Koch D., Kohfeld K. E., Prigent C., Ruedy R., Schmidt G. A., and Tegen I.: Mineral dust aerosols in the NASA Goddard Institute for Space Sciences ModelE atmospheric general circulation model, *J. Geophys. Res.*, 111, D06208, doi:10.1029/2005JD005796, 2006.
- Mishchenko, M. I., Dlugach, J. M., Yanovitskij, E. G., and Zakhrova, N. T.: Bidirectional reflectance of flat, optically thick particulate layers: an efficient radiative transfer solution and applications to snow and soil surfaces, *J. Quant. Spectrosc. Ra.*, 63, 409–432, doi:10.1016/S0022-4073(99)00028-X, 1999.
- Park, R. J., Jacob, D. J., Chin, M., and Martin, R. V.: Sources of carbonaceous aerosols over the United States and implications for natural visibility, *J. Geophys. Res.*, 108, 4355, doi:10.1029/2002JD003190, 2003.
- Park, R. J., Jacob, D. J., Field, B. D., Yantosca, R. M., and Chin, M.: Natural and transboundary pollution influences on sulfate-nitrate-ammonium aerosols in the United States: implications for policy, *J. Geophys. Res.*, 109, D15204, doi:10.1029/2003JD004473, 2004.
- Patterson, E. M., Gillet, D. A., and Stockton, B. H.: Complex index of refraction between 300 and 700 nm for Saharan aerosol, *J. Geophys. Res.*, 82, 3153–3160, doi:10.1029/JC082i021p03153, 1977.
- Prospero, J. M., Ginoux, P., Torres, O., Nicholson, S., and Gill, T.: Environmental characterization of global sources of atmospheric soil dust derived from the Nimbus 7 Total Ozone Mapping Spectrometer (TOMS) absorbing aerosol product, *Rev. Geophys.*, 40, 1002, doi:10.1029/2000RG000095, 2002.
- Ramanathan, V., Ramana, M. V., Roberts, G., Kim, D., Corrigan, C., Chung, C., and Winker, D.: Warming trends in Asia amplified by brown cloud solar absorption, *Nature*, 448, 575–578, doi:10.1038/nature06019, 2007.
- Ridley, D. A., Heald, C. L., and Ford, B.: North African dust export and deposition: a satellite and model perspective, *J. Geophys. Res.*, 117, D02202, doi:10.1029/2011JD016794, 2012.
- Russell, P. B., Hobbs, P. V., and Stowe, L. L.: Aerosol properties and radiative effects in the United States east coast haze plume: an overview of the Tropospheric Aerosol Radiative Forcing Observational Experiment (TARFOX), *J. Geophys. Res.*, 104, 2213–2222, 1999.
- Shell, K. M. and Somerville, R. C. J.: Direct radiative effect of mineral dust and volcanic aerosols in a simple aerosol climate model, *J. Geophys. Res.*, 112, D03205, doi:10.1029/2006JD007197, 2007.

Title Page

Abstract

Introduction

Conclusions

References

Tables

Figures



Back

Close

Full Screen / Esc

Printer-friendly Version

Interactive Discussion



Improved estimate of global dust radiative forcing

L. Zhang et al.

- Sinyuk, A., Torres, O., and Dubovik O.: Combined use of satellite and surface observations to infer the imaginary part of refractive index of Saharan dust, *Geophys. Res. Lett.*, 30, 1081, doi:10.1029/2002GL016189, 2003.
- Sokolik, I. N. and Toon, O. B., Direct radiative forcing by anthropogenic mineral aerosols, *Nature*, 381, 681–683, 1996.
- 5 Su, L. and Toon, O. B.: Saharan and Asian dust: similarities and differences determined by CALIPSO, AERONET, and a coupled climate-aerosol microphysical model, *Atmos. Chem. Phys.*, 11, 3263–3280, doi:10.5194/acp-11-3263-2011, 2011.
- Tegen, I. and Fung, I.: Contribution to the atmospheric mineral aerosol load from land surface 10 modification, *J. Geophys. Res.*, 100, 18707–18726, 1995.
- Tegen, I. and Lacis A. A.: Modeling of particle size distribution and its influence on the radiative properties of mineral dust aerosol, *J. Geophys. Res.*, 101, 19237–19244, doi:10.1029/95JD03610, 1996.
- 15 Tegen I., Lacis A. A., and Fung I.: The influence on climate forcing of mineral aerosols from disturbed soils, *Nature*, 380, 419–422, 1996.
- Tegen, I., Hollrigl, P., Chin, M., Fung, I., Jacob, D., and Penner, J.: Contribution of different aerosol species to the global aerosol extinction optical thickness: estimates from model results, *J. Geophys. Res.*, 102, 23895–23915, 1997.
- 20 Uno, I., Harada, K., Satake, S., Hara, Y., and Wang, Z.: Meteorological characteristics and dust distribution of the Tarim Basin simulated by the nesting RAMS/CFORS dust model, *J. Meteorol. Soc. Jpn.*, 83A, 219–239, 2005.
- Wang, Y., Jacob, D. J., and Logan, J. A.: Global simulation of tropospheric O₃-NO_x-hydrocarbon chemistry, 1. Model formulation, *J. Geophys. Res.*, 103, 10713–10726, 1998.
- Weaver, C. J., Ginoux, P., Hsu, N. C., Chou, M.-D., and Joiner, J.: Radiative Forcing of Saharan 25 Dust: GOCART model simulations compared with ERBE data, *J. Atmos. Sci.*, 59, 736–747, 2002.
- Wesely, M. L.: Parameterization of surface resistance to gaseous dry deposition in regional-scale numerical models, *Atmos. Environ.*, 23, 1293–1304, 1989.
- 30 Wielicki, B. A., Barkstrom, B. R., Harrison, E. F., Lee, R. B., Smith, G. L., and Cooper, J. E.: Clouds and the earth's radiant energy system (CERES): an earth observing system experiment, *B. Am. Meteorol. Soc.*, 77, 853–868, 1996.

[Title Page](#)

[Abstract](#)

[Introduction](#)

[Conclusions](#)

[References](#)

[Tables](#)

[Figures](#)

◀

▶

◀

▶

[Back](#)

[Close](#)

[Full Screen / Esc](#)

[Printer-friendly Version](#)

[Interactive Discussion](#)



Title Page	
Abstract	Introduction
Conclusions	References
Tables	Figures
◀	▶
◀	▶
Back	Close
Full Screen / Esc	
Printer-friendly Version	
Interactive Discussion	



- Won, J.-G., Yoon, S.-C., Kim, S.-W., Jefferson, A., Dutton, E. G., and Holben, B.: Estimation of direct radiative forcing of Asian dust aerosols with Sun/sky radiometer and lidar measurements at Gosan, Korea, *J. Meteorol. Soc. Jpn.*, 82, 115–130, 2004.
- Yoshioka, M., Mahowald, M. N., Conley, J. A., Collins D. W., Fillmore W. D., Zender S. C., and Coleman B. D.: Impact of desert dust radiative forcing on sahel precipitation: relative importance of dust compared to sea surface temperature variations, vegetation changes, and greenhouse gas warming, *J. Climate*, 20, 1445–1467, 2007.
- Zender, C. S., Bian, H., and Newman, D.: The mineral dust entrainment and deposition (DEAD) model: description and 1990s dust climatology, *J. Geophys. Res.*, 108, 4416, doi:10.1029/2002JD002775, 2003.

Improved estimate of global dust radiative forcing

L. Zhang et al.

[Title Page](#)

[Abstract](#)

[Introduction](#)

[Conclusions](#)

[References](#)

[Tables](#)

[Figures](#)

[◀](#)

[▶](#)

[◀](#)

[▶](#)

[Back](#)

[Close](#)

[Full Screen / Esc](#)

[Printer-friendly Version](#)

[Interactive Discussion](#)



Table 1. Solar and IR forcing (W m^{-2}) at TOA and at the surface.

	Vertical profile	Solar forcing		IR forcing	
		TOA	Surface	TOA	Surface
Global	GEOS-Chem	-1.85	-3.42	0.20	0.42
	FLG	-1.73	-3.46	0.16	0.46
	Diff	-0.12	0.04	0.04	-0.04
Sahara (10° N–25° N, 10° W–40° E)	GEOS-Chem	-7.53	-22.32	1.61	5.26
	FLG	-7.74	-22.96	1.78	5.43
	Diff	0.19	0.64	-0.17	-0.17
Gobi (40° N–45° N, 90° E–110° E)	GEOS-Chem	-12.24	-27.00	1.90	4.99
	FLG	-12.37	-28.16	1.84	5.36
	Diff	0.24	1.16	0.06	-0.37
Arabian Sea (5° N–25° N, 60° E–75° E)	GEOS-Chem	-8.35	-13.47	0.32	1.10
	FLG	-9.04	-14.11	0.46	1.10
	Diff	0.69	0.64	-0.14	0.00
Eastern Asia (35° N–55° N, 120° E–150° E)	GEOS-Chem	-7.69	-11.61	0.82	1.00
	FLG	-6.63	-11.49	0.38	1.26
	Diff	-1.06	-0.12	0.44	-0.26

Improved estimate of global dust radiative forcing

L. Zhang et al.

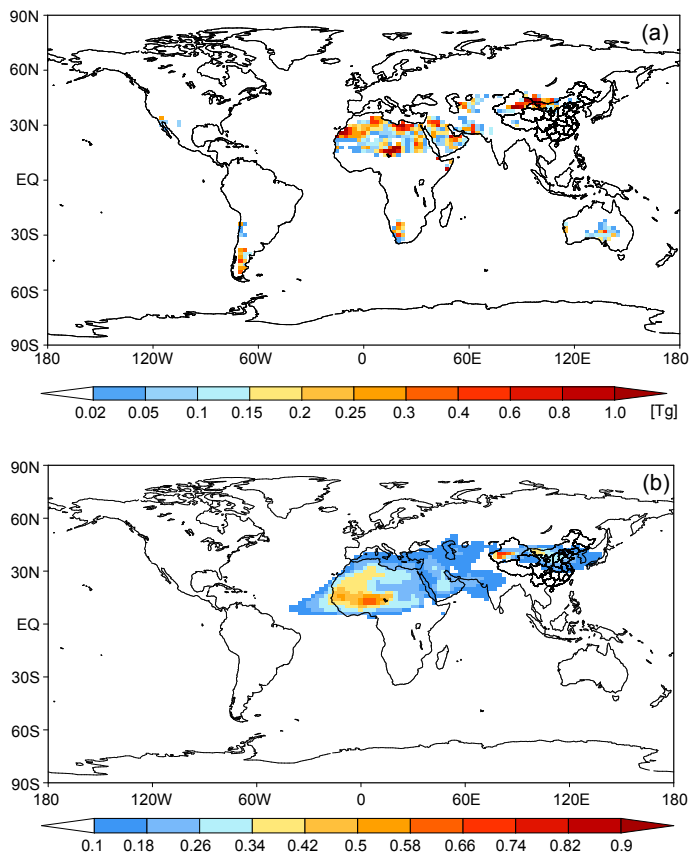


Fig. 1. GEOS-Chem simulated (a) dust emission and (b) dust AOD for April 2006.

Improved estimate of global dust radiative forcing

L. Zhang et al.

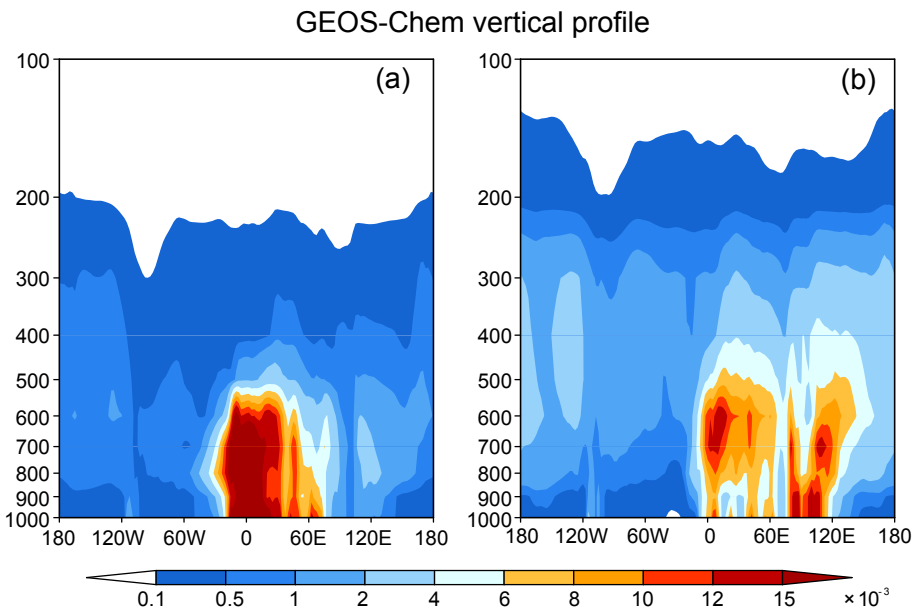


Fig. 2. Altitude-longitude cross-sections of dust AOD averaged over (a) African dust belt (10° N– 35° N) and (b) Asian dust belt (35° N– 45° N) by using GEOS-Chem vertical profile.

- [Title Page](#)
- [Abstract](#) [Introduction](#)
- [Conclusions](#) [References](#)
- [Tables](#) [Figures](#)
- [◀](#) [▶](#)
- [◀](#) [▶](#)
- [Back](#) [Close](#)
- [Full Screen / Esc](#)
- [Printer-friendly Version](#)
- [Interactive Discussion](#)



Improved estimate of global dust radiative forcing

L. Zhang et al.

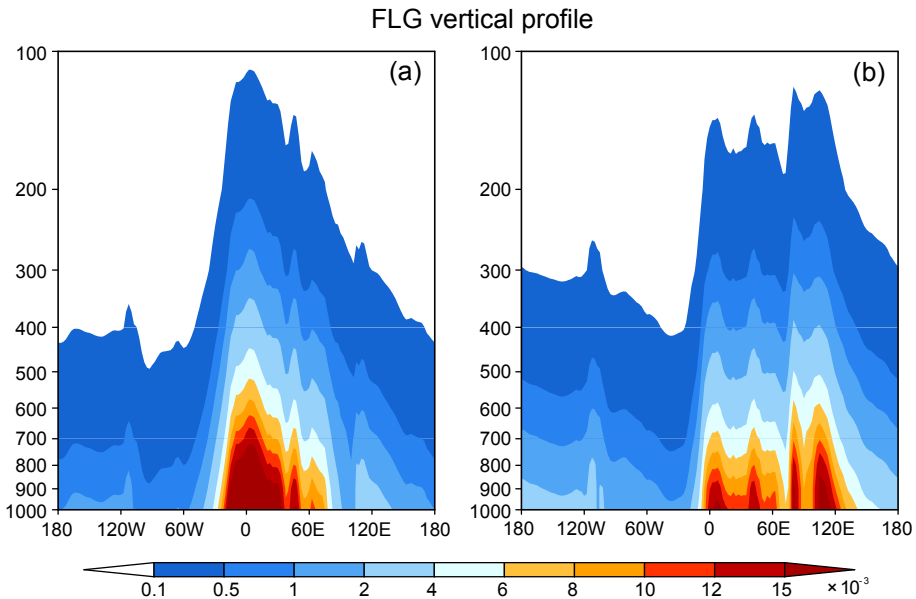


Fig. 3. Altitude-longitude cross-sections of dust AOD averaged over (a) African dust belt (10° N– 35° N) and (b) Asian dust belt (35° N– 45° N) by using FLG vertical profile.

- [Title Page](#)
- [Abstract](#) [Introduction](#)
- [Conclusions](#) [References](#)
- [Tables](#) [Figures](#)
-
-
- [Full Screen / Esc](#)
- [Printer-friendly Version](#)
- [Interactive Discussion](#)



Improved estimate of global dust radiative forcing

L. Zhang et al.

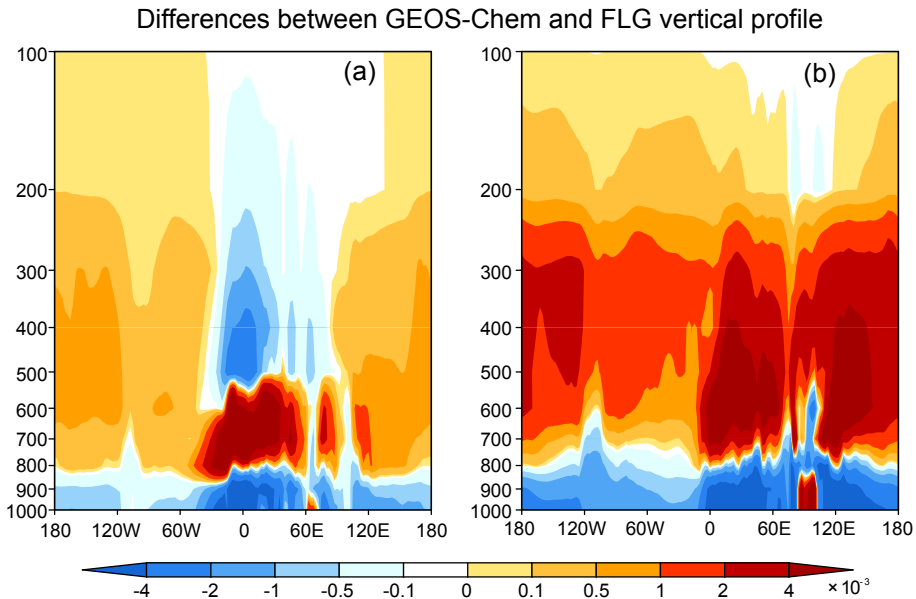


Fig. 4. Differences of dust AOD between using GEOS-Chem vertical profile and FLG vertical profile (former minus latter) averaged over **(a)** African dust belt (10° N– 35° N) and **(b)** Asian dust belt (35° N– 45° N).



Improved estimate of global dust radiative forcing

L. Zhang et al.

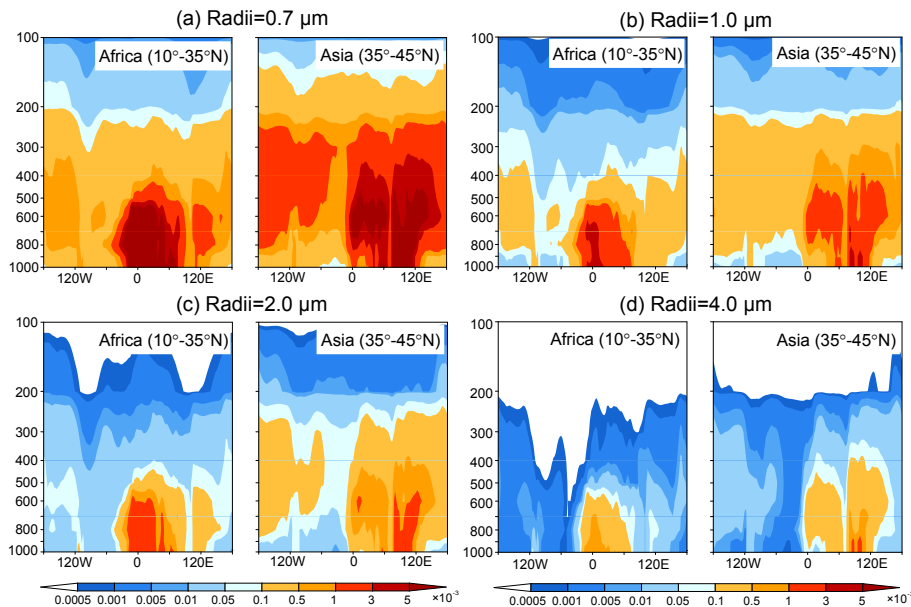


Fig. 5. Differences of dust AOD for four size bins **(a)** radii = 0.7 μm ; **(b)** radii = 1.0 μm ; **(c)** radii = 2.0 μm ; **(d)** radii = 4.0 μm between using GEOS-Chem vertical profile and FLG vertical profile (former minus latter) averaged over African dust belt (10° N–35° N) and Asian dust belt (35° N–45° N).

- [Title Page](#)
- [Abstract](#) [Introduction](#)
- [Conclusions](#) [References](#)
- [Tables](#) [Figures](#)
- [◀](#) [▶](#)
- [◀](#) [▶](#)
- [Back](#) [Close](#)
- [Full Screen / Esc](#)
- [Printer-friendly Version](#)
- [Interactive Discussion](#)



Improved estimate of global dust radiative forcing

L. Zhang et al.

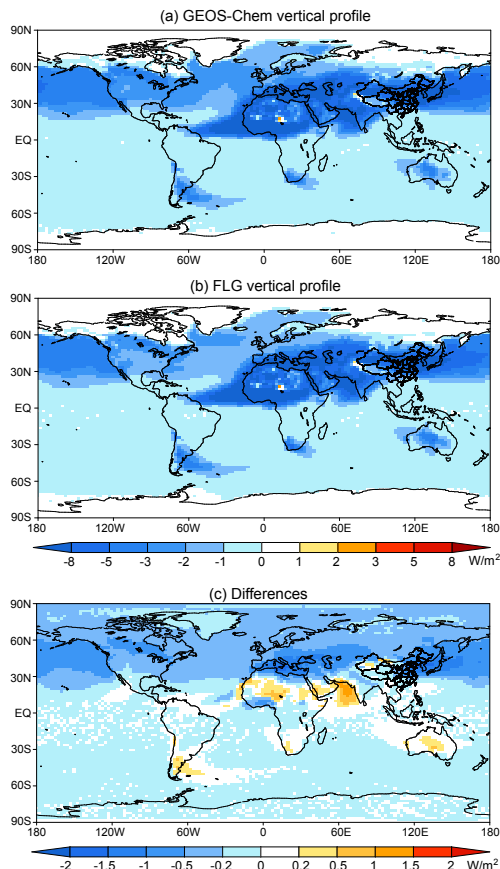


Fig. 6. Solar radiative forcing at the TOA with **(a)** GEOS-Chem vertical profile; **(b)** FLG vertical profile; and **(c)** differences between using GEOS-Chem vertical profile and FLG vertical profile (former minus latter).

[Title Page](#)[Abstract](#)[Introduction](#)[Conclusions](#)[References](#)[Tables](#)[Figures](#)[Back](#)[Close](#)[Full Screen / Esc](#)[Printer-friendly Version](#)[Interactive Discussion](#)

Improved estimate of global dust radiative forcing

L. Zhang et al.

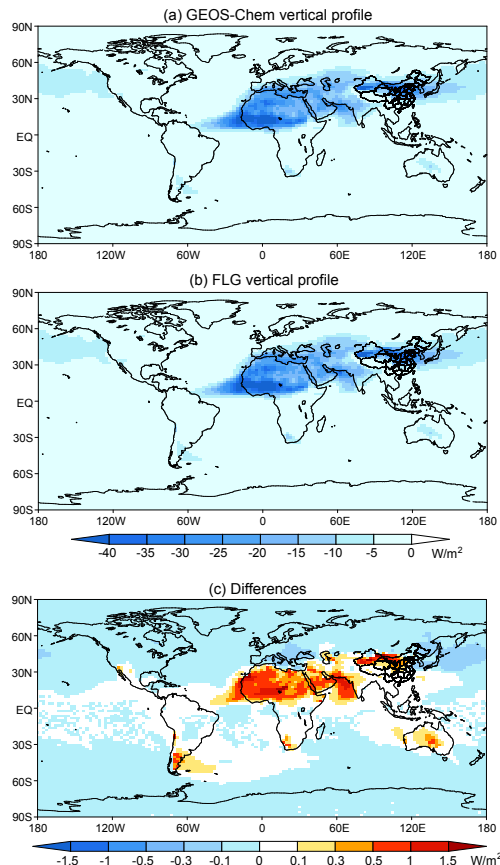


Fig. 7. Solar radiative forcing at the surface with **(a)** GEOS-Chem vertical profile; **(b)** FLG vertical profile; and **(c)** differences between using GEOS-Chem vertical profile and FLG vertical profile (former minus latter).

[Title Page](#)[Abstract](#)[Introduction](#)[Conclusions](#)[References](#)[Tables](#)[Figures](#)[Back](#)[Close](#)[Full Screen / Esc](#)[Printer-friendly Version](#)[Interactive Discussion](#)

Improved estimate of global dust radiative forcing

L. Zhang et al.

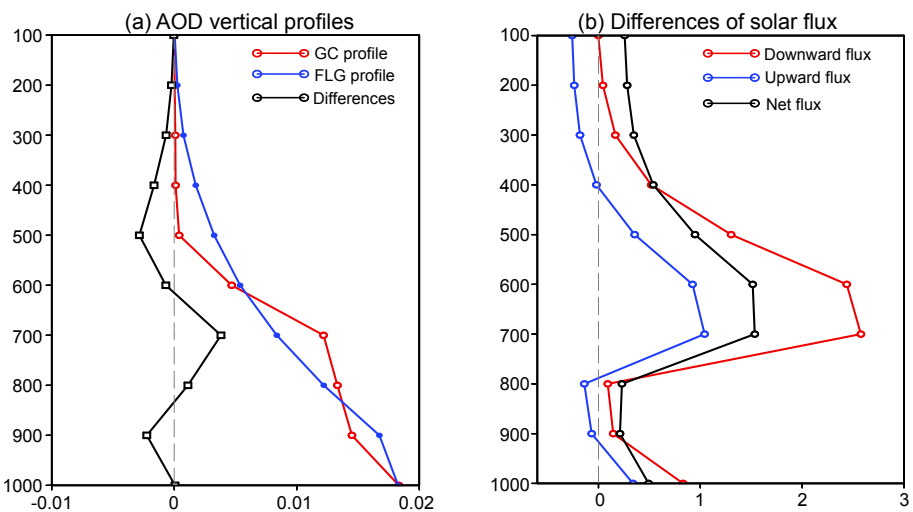


Fig. 8. Vertical profiles of (a) dust AOD and (b) the differences of dust solar radiative flux at the location of Sahara desert (10° E, 20° N).

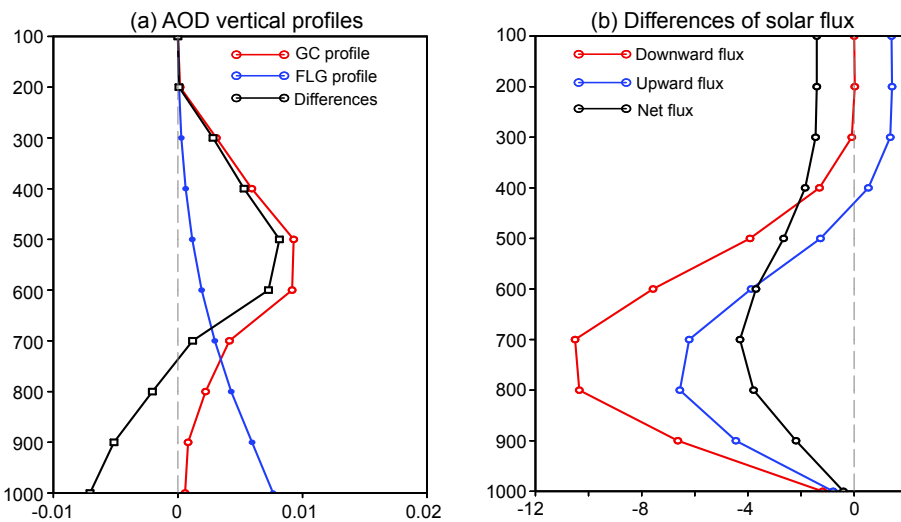


Fig. 9. Same as Fig. 8, but at the location of Eastern Asia (140° E, 40° N).

Improved estimate of global dust radiative forcing

L. Zhang et al.

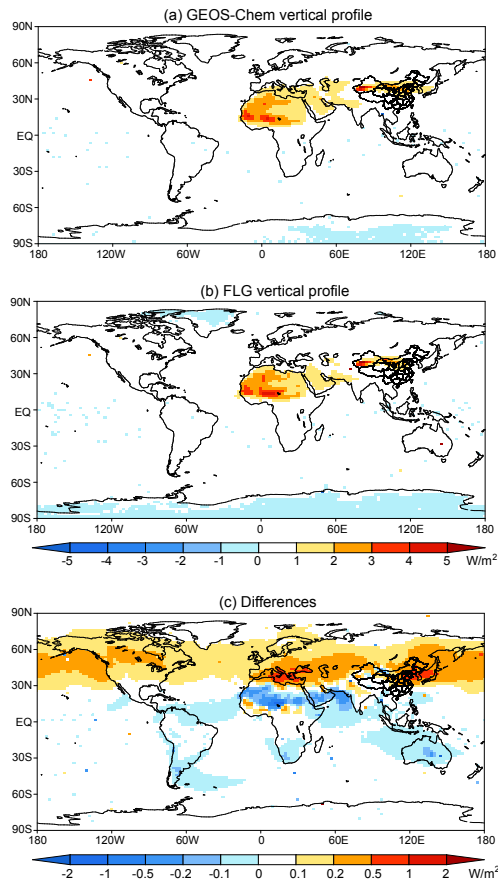


Fig. 10. IR radiative forcing at the TOA with **(a)** GEOS-Chem vertical profile; **(b)** FLG vertical profile; and **(c)** differences between using GEOS-Chem vertical profile and FLG vertical profile (former minus latter).

[Title Page](#)[Abstract](#)[Introduction](#)[Conclusions](#)[References](#)[Tables](#)[Figures](#)[Back](#)[Close](#)[Full Screen / Esc](#)[Printer-friendly Version](#)[Interactive Discussion](#)

Improved estimate of global dust radiative forcing

L. Zhang et al.

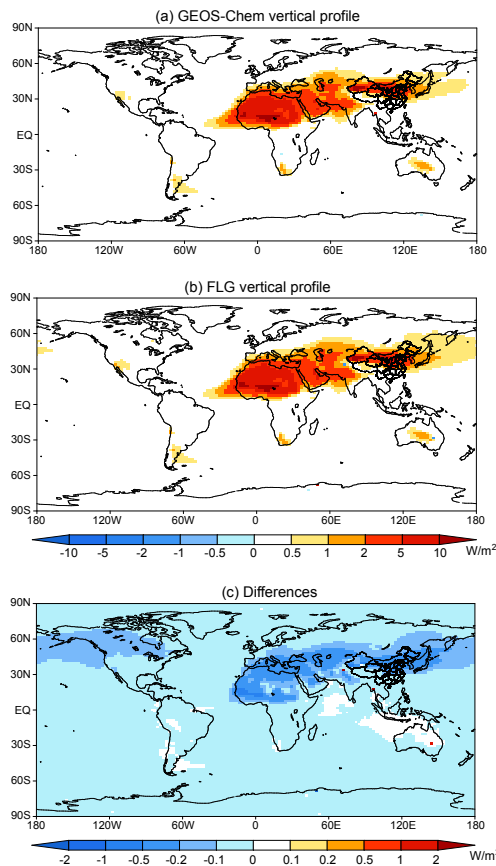


Fig. 11. IR radiative forcing at the surface with (a) GEOS-Chem vertical profile; (b) FLG vertical profile; and (c) differences between using GEOS-Chem vertical profile and FLG vertical profile (former minus latter).

[Title Page](#)[Abstract](#)[Introduction](#)[Conclusions](#)[References](#)[Tables](#)[Figures](#)[Back](#)[Close](#)[Full Screen / Esc](#)[Printer-friendly Version](#)[Interactive Discussion](#)

Improved estimate of
global dust radiative
forcing

L. Zhang et al.

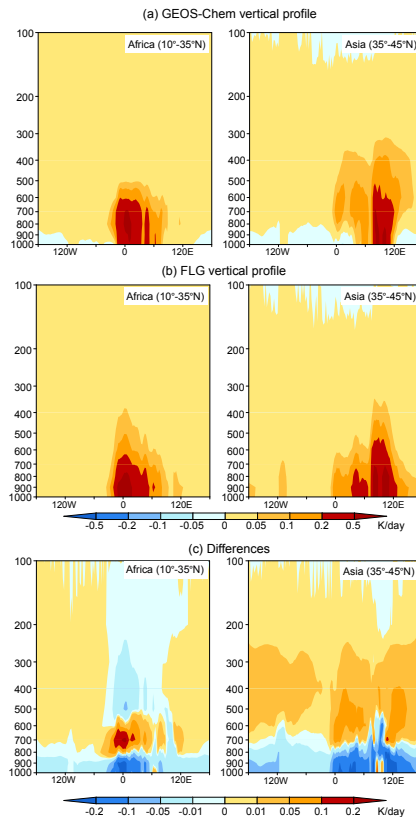


Fig. 12. Altitude-longitude cross-sections of solar heating rate due to dust with **(a)** GEOS-Chem vertical profile; **(b)** FLG vertical profile; and **(c)** differences between using GEOS-Chem vertical profile and FLG vertical profile (former minus latter) averaged over African dust belt (10° N– 35° N) and Asian dust belt (35° N– 45° N).

[Title Page](#)[Abstract](#)[Introduction](#)[Conclusions](#)[References](#)[Tables](#)[Figures](#)[|◀](#)[▶|](#)[◀](#)[▶](#)[Back](#)[Close](#)[Full Screen / Esc](#)[Printer-friendly Version](#)[Interactive Discussion](#)

Improved estimate of global dust radiative forcing

L. Zhang et al.

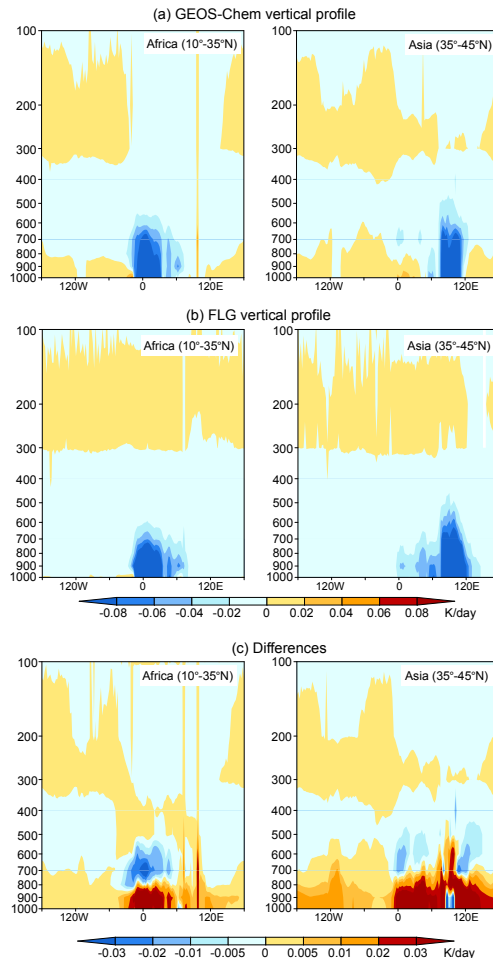
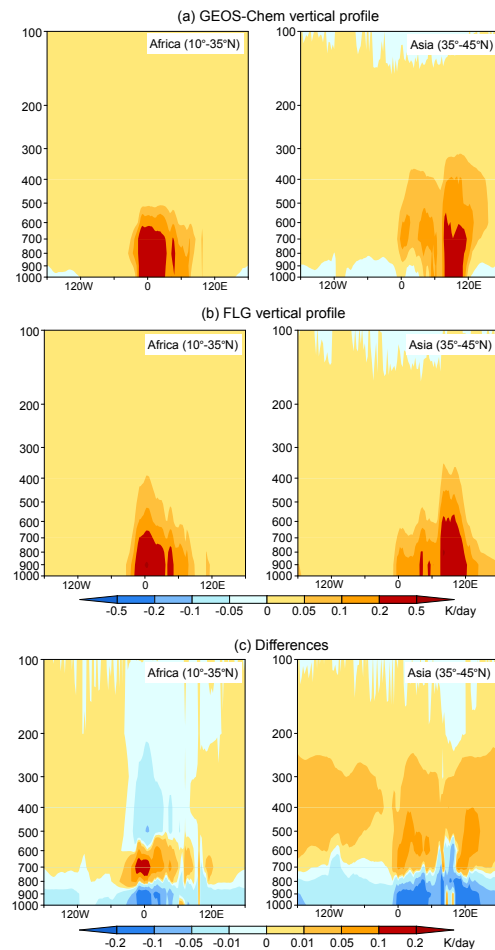


Fig. 13. Same as Fig. 12, but for IR heating rate due to dust.

Improved estimate of global dust radiative forcing

L. Zhang et al.

**Fig. 14.** Same as Fig. 12, but for net heating rate due to dust.